Journal of Physics and Chemistry of Solids 74 (2013) 70–74

Contents lists available at SciVerse ScienceDirect

Journal of Physics and Chemistry of Solids

journal homepage: www.elsevier.com/locate/jpcs

Effect of KOH on glycine phosphite single crystal grown by the SR method

S. Supriya [a], S. Kalainathan [a,*], G. Bhagavannarayana [b]

[a] School of Advanced Sciences, VIT University, Vellore 632014, India
[b] Materials Characterization Division, National Physical Laboratory(CSIR), New Delhi 110 012, India

ARTICLE INFO

Article history:
Received 9 September 2010
Received in revised form
24 June 2012
Accepted 5 August 2012
Available online 25 August 2012

Keywords:
B. Crystal growth
C. Infrared spectroscopy
C. X-ray diffraction

ABSTRACT

The pure glycine phosphite (pure-GPI) and a new potassium hydroxide doped glycine phosphite (KOH-GPI) single crystals have been grown from aqueous solution by slow evaporation and Sankaranarayanan and Ramasamy method (SR method). The colorless KOH-GPI crystal with cylindrical shape about 15 mm diameter and 49 mm length was obtained by the SR method. The formation of KOH-GPI has been confirmed by single crystal X-ray diffraction by comparing with pure GPI. Its crystalline perfection was assessed by High resolution X-ray diffraction (HRXRD) studies. The fourier transform infrared spectroscopy (FTIR) studies and UV–visible transmission and absorption spectrum analysis were carried out for KOH-GPI and it is compared with pure GPI. From the dielectric studies, at the frequency value of 1000 KHz, the curie temperature of pure GPI and KOH-GPI was found to be 228.44 and 240.90 K respectively. The KOH-GPI shows high curie temperature value comparing with pure GPI. The results will be discussed in detail.

1. Introduction

The hydrogen bonded crystal Glycine phosphite ($NH_3CH_2COOH_3PO_3$) abbreviated as GPI, and betanine phosphite crystal [$(CH_3)_3NCH_2COOH_3PO_3$] abbreviated as BPI shows ferroelectric nature with ordering of protons in their structure. In low temperature phase the proton ordering is expected along its *c*-axis and the spontaneous polarization is parallel to the monoclinic *b*-axis [1–4]. The similar situation is observed in KDP family of crystals where hydrogen bonds are perpendicular to the ferroelectric axis [5]. The GPI crystal belongs to monoclinic system with space group P21/a and cell parameters of $a=9.792$ Å, $b=8.487$ Å and $c=7.411$ Å and $\beta=100.43^\circ$ [6,7] and also the crystal undergoes continuous ferroelectric to para-electric phase transition at 224 K which was already reported by dielectric measurements. To understand this ferroelectric phase transition mechanism, several investigations were carried out by various research groups [8–10].

The Sankaranaryanan and Ramasamy (SR) method is one of the new unidirectional crystal growth methods which offers simple solution growth at room temperature with less sophisticated equipment and gives cylindrical morphology. The major advantage of this method is the easy scaling up of diameter and has nearly 100% solute-crystal efficiency. It does not give problems like thermal decompositions [11–14]. This method has high growth rate, yield defect free transparent bulk single crystals along a particular axis and prevents from microbial growth [15–18].

However, no growth details with the addition of potassium hydroxide (KOH) with GPI have been reported so far. And also the investigations on the SR method of this crystal have not been reported yet. Hence in this paper we report a detailed comparative study of the growth and characterization of pure GPI and KOH-GPI crystal by the SR method.

2. Experimental procedure

2.1. Method of material synthesis

Glycine phosphite ($NH_2CH_2COOH_3PO_3$) was synthesized by dissolving equimolar ratio of high purity glycine [NH_2CH_2COOH] (AR grade) and orthophosphorous acid [H_3PO_3] (Sigma Aldrich), with millipore water as the solvent.

The following reaction is expected to take place with the formation of the glycine phosphate:

$$NH_2CH_2COOH + H_3PO_3 \rightarrow NH_3CH_2COO \cdot H_3PO_3 \quad (1)$$

After complete dissolvation of these two compounds 5 mol% of potassium hydroxide (KOH) was added as a dopant material in this solution. Again solution was stirred very well to obtain complete dissolvation. Then the temperature of the solution is decreased to room temperature. By keeping the solution into refrigerator, it was cooled to temperature about 0 °C. The temperature of the solution

* Corresponding author. Tel.: +91 416 2202350; fax: +91 416 2243092.
E-mail addresses: ssupriya495@gmail.com (S. Supriya), kalainathan@yahoo.com (S. Kalainathan), bhagavan@mail.nplindia.ernet.in (G. Bhagavannarayana).

0022-3697/$ - see front matter © 2012 Elsevier Ltd. All rights reserved.
http://dx.doi.org/10.1016/j.jpcs.2012.08.001

was decreased gradually so that we can obtain potassium hydroxide doped glycine phosphite (KOH-GPI) powder crystals. The complete precipitation and proper filtering has been done to dry the KOH-GPI powder crystals. To get purified material and good quality crystals the KOH-GPI synthesized salt was recrystallized several times.

By employing the slow evaporation method, the fine crystals of KOH-GPI were obtained from saturated solution. Pure GPI crystals were also grown similarly by slow evaporation and SR methods (the following method) without adding potassium hydroxide.

Figs. 1 and 2 shows single crystals of pure and KOH doped GPI and which are obtained by slow evaporation method respectively. The morphology of pure-GPI (Fig. 1) consists crystal habit of {011}, {010}, {100}, {110}, {111} and {211}faces [19].

The change in morphology of KOH-GPI was observed comparing with pure GPI which is shown in Fig. 2. The morphology of KOH-GPI mainly consists crystal habit of {110}, {013} faces and some of other faces also which is shown in the figure.

2.2. Growth of KOH-GPI by the SR method

The saturated solution of KOH-GPI was transferred into 15 mm diameter cylindrical shape growth ampoule. The KOH-GPI crystal which is obtained by slow evaporation method was inserted into the growth ampoule. The bottom of growth ampoule was closed. The temperature around the growth ampoule was controlled by the temperature controller. The growth of crystal was observed continuously and it was allowed to grow for required length under proper condition.

Under controlled condition, the highly transparent crystal with size of 15 mm diameter and 49 mm length was obtained in a couple of months. Fig. 3 shows the colorless, cylindrical shape, good quality of unidirectional KOH-GPI single crystal harvested by the SR method.

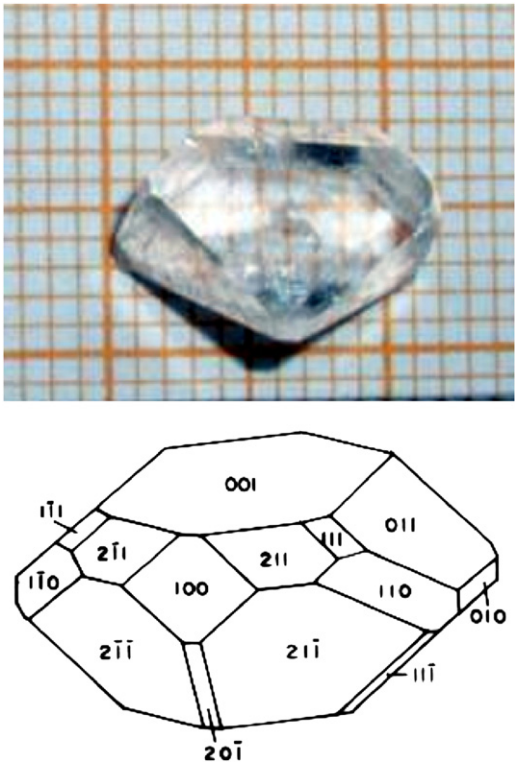

Fig. 1. Pure-GPI single crystal by the slow evaporation method and its morphology.

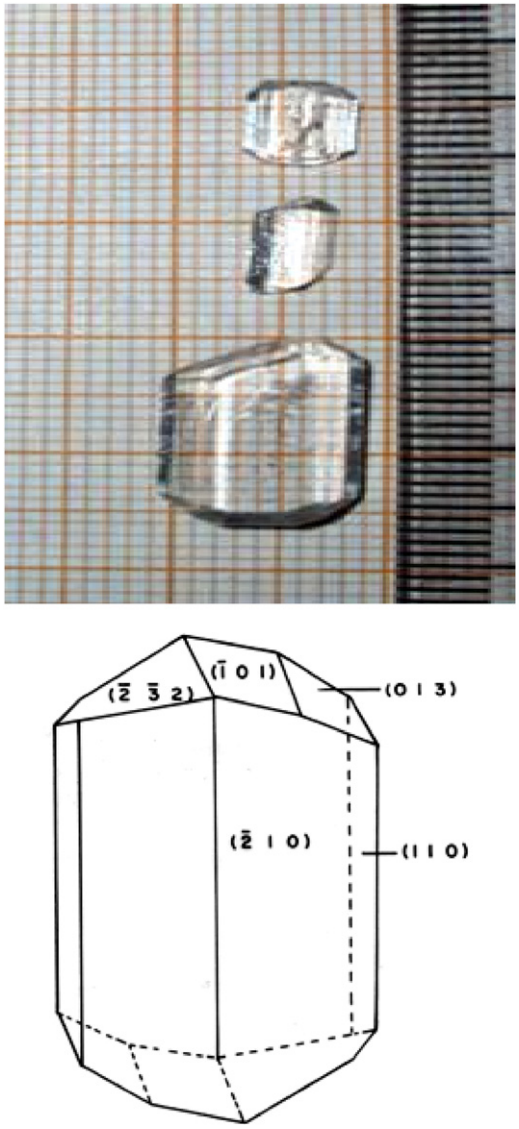

Fig. 2. KOH-GPI single crystal by the slow evaporation method and its morphology.

Fig. 3. KOH-GPI crystal by the SR method.

3. Characterization studies

The single crystal X-ray diffraction analysis (by using ENRAF NONIUS CAD4 diffractometer) was carried out for the grown

crystal. The high-resolution X-ray diffraction (HRXRD) curve has been recorded for single crystal specimen by employing the multicrystal X-ray diffractometers. The FTIR spectra samples were recorded by KBr pellet method by using Avatar 330 FTIR thermo Nicolet spectrometer. The UV–visible spectrum was recorded on a HITACHI model U-2800 double beam spectrophotometer in the wavelength range from 200 to 900 nm.

4. Results and discussion

4.1. Single crystal X-ray diffraction analysis

The Table 1 shows the lattice parameter values of pure GPI and KOH-GPI. The single crystal X-ray diffraction analysis of pure and KOH-GPI exhibits monoclinic crystal system. Comparing with pure GPI, the KOH GPI shows there is decrease of lattice parameters values due to the addition of KOH in GPI.

Table 1
The lattice parameter values of pure GPI and KOH-GPI.

	a (Å)	b (Å)	c (Å)	β (°)
Pure GPI	9.782	8.482	7.402	100.33
KOH-GPI	9.740	8.453	7.407	100.06

$\alpha=\gamma=90°$, volume=605.19 Å and system=monoclinic.

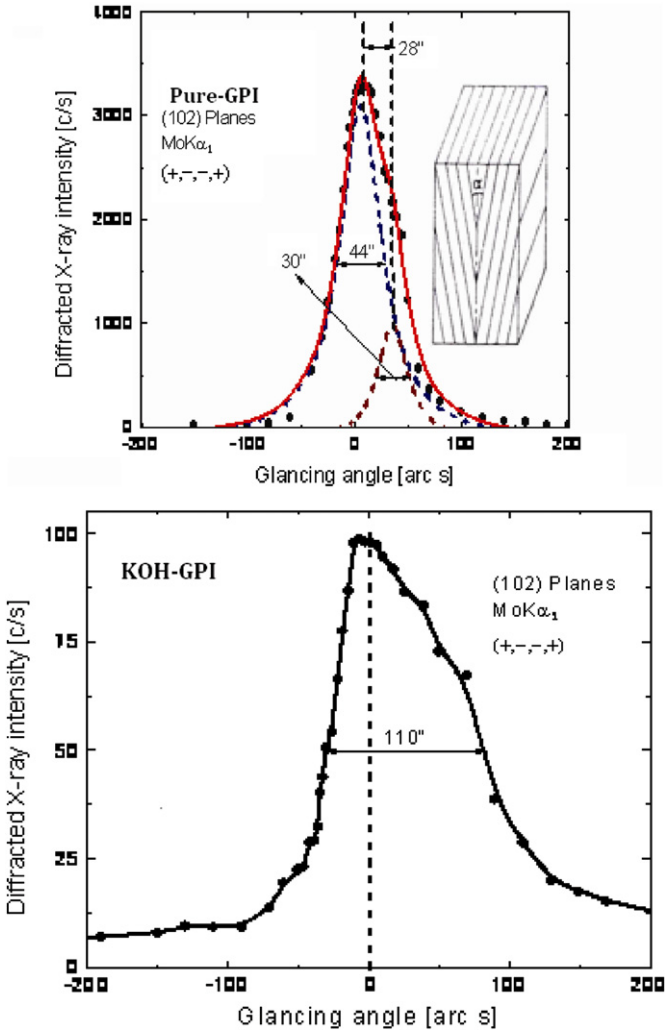

Fig. 4. HRXRD of pure GPI and KOH-GPI.

4.2. High resolution X-ray diffraction analysis (HRXRD)

Fig. 4 shows the high-resolution X-ray diffraction curve (DC) recorded for a pure GPI and KOH-GPI single crystals specimen using (102) diffracting planes in a symmetrical Bragg geometry by employing the multicrystal X-ray diffractometer. In the HRXRD of pure GPI, the solid line (convoluted curve) is well fitted with the experimental points represented by the filled circles. On deconvolution of the diffraction curve, it is clear that the curve contains an additional peak, which is 28 arcs away from the main peak. This additional peak depicts an internal structural very low angle (tilt angle ≤ 1 arcmin) boundary. As seen in the HRXRD of KOH-GPI, the DC contains a single peak and indicates that the specimen is free from structural grain boundaries. The full width at half maximum (FWHM) of these curve is 110 arcs which is quite higher than that expected from the plane wave theory of dynamical

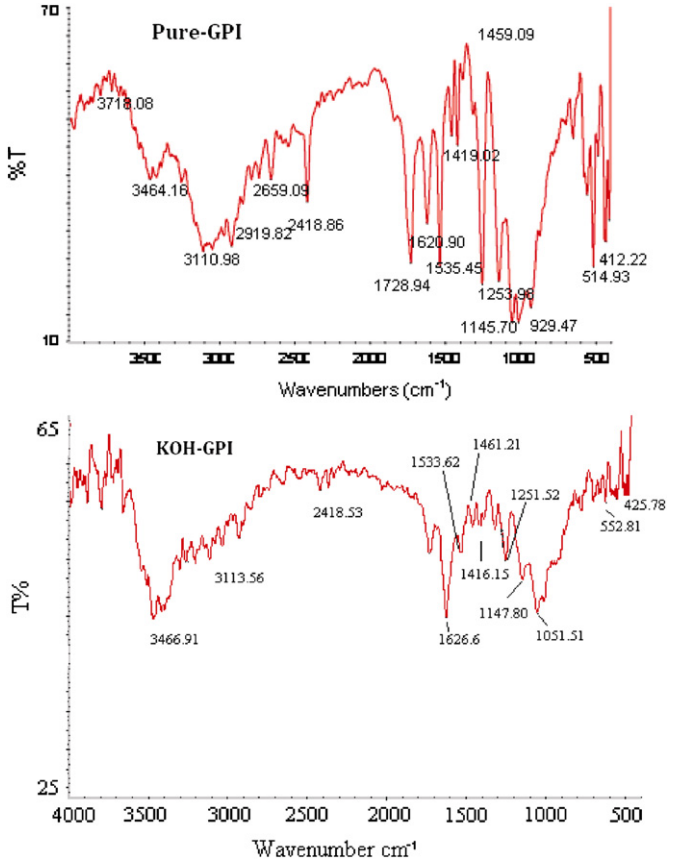

Fig. 5. FTIR spectra of pure and KOH doped GPI.

Table 2
Comparison of the main IR Aspectral data (cm^{-1}) of pure GPI and KOH-GPI.

S. no.	Assignment	pure-GPI	KOH-GPI
1	υ_s (COO^-)	1419.02	1416.15
2	υ_a (COO^-)	1620.90	1626.60
3	δ (COO^-)	514.93	552.81
4	δ_s (NH_3^+)	1459.09	1461.21
5	ρ_r (COO^-)	412.22	425.78
6	ρ_r (NH_3^+)	1145.70	1147.80

X-ray diffraction for an ideally perfect crystal [20], but close to that expected for nearly perfect real life crystals. This much broadness with good scattered intensity along the wings of the DC indicates that the crystal contains point defects and their aggregates. Such defects are very common to observe in almost all real crystals including nature gifted crystals and are many times unavoidable due to thermo dynamical conditions [20].

It is interesting to see the shape of the DC. As seen in the figure, the DC is not symmetric with respect to the Bragg peak position, which indicates that the density of vacancy and interstitial defects are not same. For a particular angular deviation ($\Delta\theta$) of glancing angle (θ) with respect to the Bragg peak position (taken as zero for the sake of convenience), the scattered intensity is much more in the positive direction in comparison to that of the negative direction. This feature clearly indicates that the crystal contains predominantly interstitial type of defects than that of vacancy defects. This can be well understood by the fact that due to interstitial defects (self interstitials or impurities or dopants at interstitial sites), the lattice around these defects undergo compressive stress and the lattice parameter d (interplanar spacing) decreases close to the defect core and leads to give more scattered (also known as diffuse X-ray scattering) intensity at slightly higher Bragg angles (θ_B) as d and $\sin\theta_B$ are inversely proportional to each other in the Bragg equation ($2d\sin\theta_B = n\lambda$; n and λ being the order of reflection and wavelength respectively which are fixed). The inset in the curve shows the schematic to illustrate how the lattice around the defect core undergoes compressive stress. The converse explanation is true in case of vacancy defects which cause tensile stress in the lattice around the defect core leading to increase of lattice spacing and in turn results in more scattered intensity at the lower Bragg angles. However, the single diffraction curve with reasonably low FWHM indicates that the crystalline perfection is fairly good. The density of such interstitial defects is however meager and in almost all real crystals including nature gifted crystals, such defects are commonly observed and are many times unavoidable due to thermo dynamical conditions and hardly affect the device performance [21,22] which is however not the main focus of the present investigation.

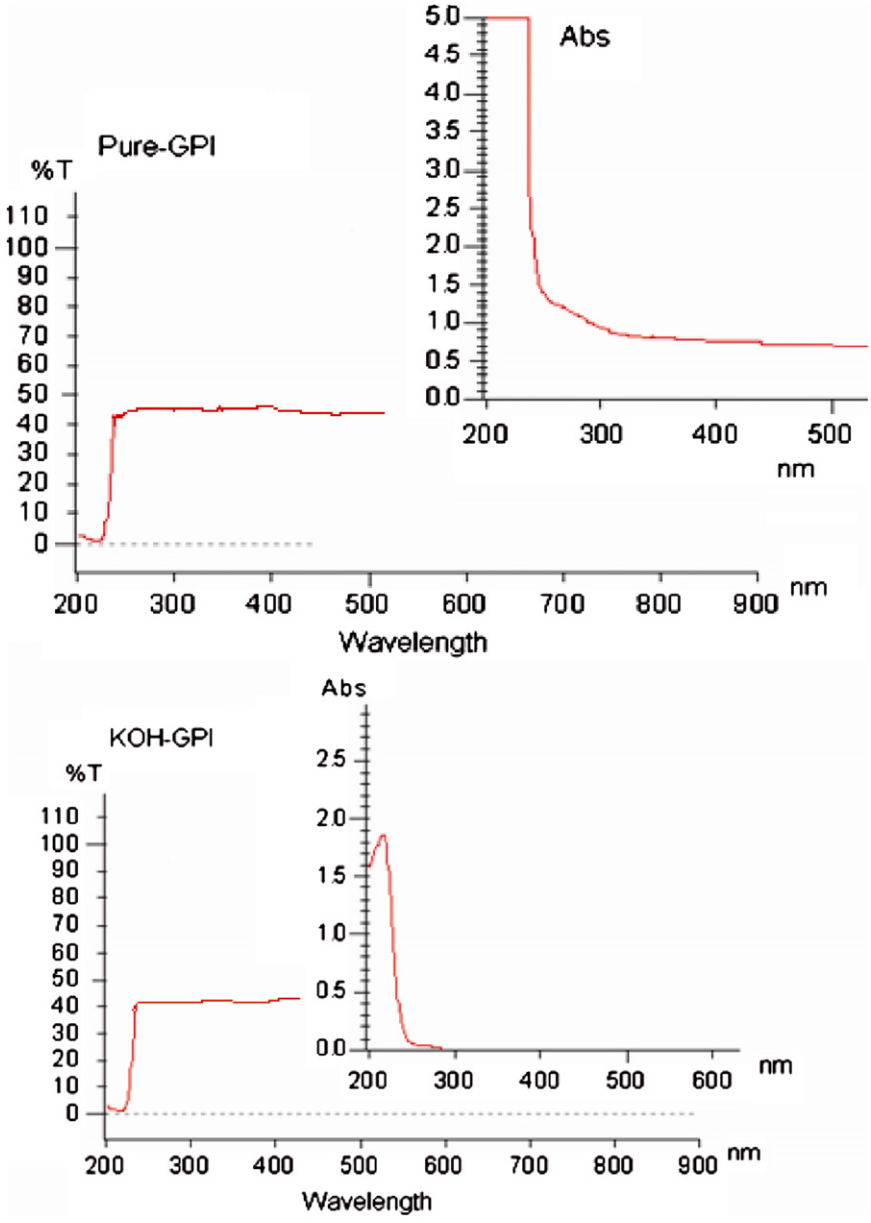

Fig. 6. UV–visible transmission and absorption spectrum.

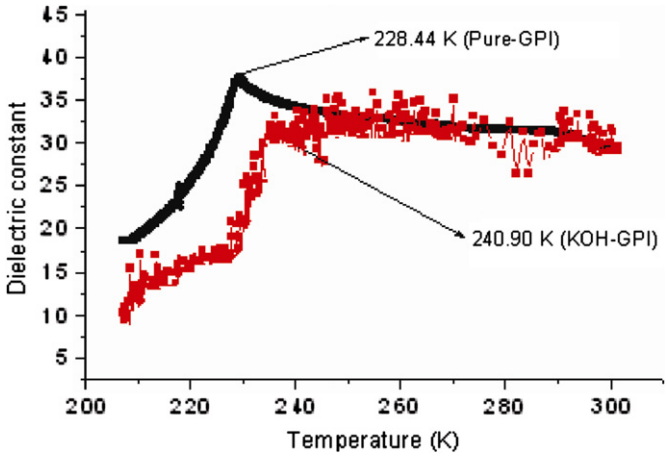

Fig. 7. Variation of dielectric constant with temperature of pure and KOH-GPI at 1000 KHz.

It is worth to mention here that the observed scattering due to point defects is of short range order as the strain due to such minute defects is limited to the very defect core and the long range order could not be expected and hence the change in the lattice parameter of the overall crystal is not expected.

4.3. FTIR analysis

The graphs of FTIR spectrum of pure GPI and KOH-GPI are shown in Fig. 5. The IR spectral datas of KOH-GPI is compared with pure GPI values which are shown in Table 2. Comparing with pure GPI, the KOH-GPI shows there is disappearance of many peaks at the wave numbers of 1253.98, 1728.94, 2418.86, 2919.82 cm^{-1}. The value of symmetric stretching vibration of COO^- decreases with pure GPI. The anti symmetric stretching and bending vibrations shows high value in KOH-GPI crystal. The rocking vibration of COO^- decreases and NH_3^+ increases. All these confirm the presence of potassium hydroxide in glycine phosphite.

4.4. UV–visible transmission and absorption spectrum

The UV–visible transmission and absorption spectrum of pure GPI and KOH-GPI were recorded at the wavelength range of 200–900 nm by dissolving the powder sample in ethanol and water in 1:1 ratio (Fig. 6) and there is no significant change observed in cut off wavelengths of transmission spectrum for both the samples. But in case of absorption spectrum small change has been observed. Absences of absorption regions were observed between 300 and 900 nm for both the samples.

4.5. Dielectric studies

The transparent good quality crystal is polished well using alumina powder and paraffin oil to study the dielectric property. The silver paste was applied on both the opposite surfaces of the crystal which acted as electrodes. The chamber is filled with helium gas and dielectric response is measured for the frequency of 1000 KHz for the pure GPI and KOH-GPI. The temperature is controlled from 205 to 303 K by using a computer keithley nano voltmeter relay arrangement up to accuracy of 0.1 K. Measurements are recorded and the almost similar variation was observed for other frequencies also for the both the samples. So the graph is plotted for 1000 KHz only.

It has been reported already that for the pure GPI, the measured value of dielectric constant is at the transition temperature of 224 K for a frequency value of 10 KHz [23]. But for the frequency value of 1000 KHz we found that the phase transition temperature of pure GPI is at 228.44 K and the KOH-GPI's phase transition temperature was compared with this value. The curie temperature of KOH-GPI was found at 240.90 K.

Fig. 7 shows the dielectric constant values and the phase transition temperature of pure GPI and KOH-GPI. After adding 5 mol% of potassium hydroxide in glycine phosphite, it was observed that the curie temperature of crystal was slightly increased. This result confirms the presence of KOH in glycine phosphite.

5. Conclusions

The pure GPI and 5 mol% KOH added GPI single crystals were grown by SR method. The crystalline quality and lattice parameters of pure and KOH-GPI were compared by single crystal, and powder X-ray diffraction analysis. The high resolution X-diffraction results were briefly discussed for both the crystals. This brief analysis of HRXRD data promises the effect of potassium hydroxide in glycine phosphite. The functional groups were analyzed by FTIR spectroscopy for both the samples. The optical properties were observed by UV–visible spectrum. The curie temperature of pure GPI and KOH-GPI has been determined by using dielectric studies.

Acknowledgments

Authors are thankful to management of VIT University, Vellore and the Director, National Physical Laboratory, New Delhi for their constant encouragement and financial support.

References

[1] C.Preethy Menon, J. Philip, A. Deepthy, H.L. Bhat, Mater. Res. Bull. 36 (2001) 2407–2414.
[2] J. Tritt-Goc, N. Pislewski, L. Szczepanska, Solid State Commun. 108 (1998) 189–192.
[3] M. Sledź, J. Baran, J. Mol. Struct. 706 (2004) 15–48.
[4] J. Goslar, S.K. Hoffmann, W. Hilczer, Solid State Commun. 121 (2002) 423–427.
[5] M.E. Lines, A.M. Glass, Principles and Application of Ferroelectric and Related Materials, third ed., Clarendon Press, Oxford, 1977.
[6] J. Baran, K. Lukaszewicz, A. Pietraszko, M. Sledz, J. Mol. Struct. 611 (2002) 155–168.
[7] R. Perumal, K.Senthil Kumar, S.Moorthy Babu, G. Bhagavannarayana, J. Alloys Compd. 490 (2010) 342–349.
[8] T. Kanagasekaran, P. Mythili, G. Bhagavannarayana, D. Kanjilal, R. Gopalakrishnan, Beam Interact. Mater. At. 267 (2009) 2495–2502.
[9] M.M. Khandpekar, S.P. Pati, Opt. Commun. 283 (2010) 2700–2704.
[10] D.S Chemla, J. Zyss, Nonlinear Optical Properties of Organic Materials and Crystals, third ed., Academic Press, New York, 1979.
[11] A. Senthil, P. Ramasamy, J. Cryst. Growth 311 (2009) 4720–4724.
[12] A. Senthil, R.Ramesh Babu, N. Balamurugan, P. Ramasamy, J. Cryst. Growth 311 (2009) 544–554.
[13] R.Ramesh Babu, K. Sethuraman, R. Gopalakrishnan, J. Cryst. Growth 297 (2006) 356–360.
[14] R.Bairava Ganesh, V. Kannan, R. Sathyalakshmi, P. Ramasamy, Mater. Lett. 61 (2007) 706–708.
[15] K. Sankaranaryanan, P. Ramasamy, J. Cryst. Growth 292 (2006) 445–448.
[16] K. Sankaranaryanan, J. Cryst. Growth 284 (2005) 203–208.
[17] C.Justin Raj, S. Dinakaran, S. Krishnan, B.Milton Boaz, R. Robert, S.Jerome Das, Opt. Commun. 281 (2008) 2285–2290.
[18] P. Ramasamy, J. Cryst. Growth 310 (2008) 1501–1504.
[19] J. Nayeem, T. Kikuta, T. Yamazaki, N. Nakatani, Jpn. J. Appl. Phys. 39 (2000) 6612–6613.
[20] M. Jose, G. Bhagavannarayana, K. Sugandhi, S.Jerome Das, Mater. Lett. 64 (2010) 1369–1371.
[21] G. Bhagavannarayana, S.K. Kushwaha, S. Parthiban, Subbiah Meenakshisundaram, J.Cryst. Growth 311 (2009) 960–965.
[22] G. Bhagavannarayana, S.K. Kushwaha, S. Parthiban, G. Ajitha, Subbiah Meenakshisundaram, J. Cryst. Growth 310 (2008) 2575–2583.
[23] R.Ezhil Vizhi, S. Kalainathan, G.Baghavan Narayana, Cryst. Res. Technol. 42 (2007) 1104–1109.